Different Control Strategies for Power Control of Voltage Source Converters in a Microgrid

Er. Shashank S. Deshmukh[1], Er. Shridhar S. Khule[2]

[1]PG student, Department of Electrical Engineering, Matoshri College of Engineering and Research Centre, Eklahare, Nashik, Maharashtra, India.
[2]Head of Department, Department of Electrical Engineering, Matoshri College of Engineering and Research Centre, Eklahare, Nashik, Maharashtra, India.

---***---

Abstract - *Traditional proportional integral (PI) control has been extensively used for power control of voltage source converters in microgrid systems. A new Critic based PI controller is discussed in this paper. In another method using the PR controllers, the converter reference tracking performance can be enhanced and previously known shortcomings associated with conventional PI controllers can be alleviated. Another control strategy includes Vector controlled VSC's. In it the main improvement is to suppress the possible dc-link voltage fluctuations under power line faults and unbalanced conditions. Another control strategy includes Hysteresis Current Controller employed for the inverter control. The proposed inverter control technique interfaces renewable energy sources and the AC bus of micro grid. It offers the possibility to inject power from the renewable sources and also improves the power quality in the same micro grid. Also a vector control strategy for regulating the current of grid-tied voltage source converters in a rotating reference frame is suggested in this paper.*

Key Words: fuzzy logic, proportional-resonant (PR) controllers, High-voltage direct current (HVDC), Lyapunov methods, pulse width modulation (PWM), RTDS, vector-controlled VSC, Synchronous Reference Frame, DQ-Current Control, Voltage Source Converters.

I. INTRODUCTION

A microgrid is an integration of multiple distributed energy resources such as generation, storage, and load units at the distribution level. This single united system is capable of operating in both grid-connected and stand-alone or islanded modes. The nature of most distributed energy resources in the microgrid requires power electronic-based converters to reshape their generated energy to a form compatible with the utility grid's voltage and frequency. The majority of DGs are hence interfaced to the microgrid through voltage source converters (VSCs). Furthermore, compared to traditional electric machines, use of power electronic converters yields to more operation and control flexibility for the microgrid sources. Nevertheless, it should be noted that the lower physical inertia of power electronic converters leads to higher sensitivity to the network disturbances and may in occasions result in power oscillations and violation of overall stability. Power control of VSCs has been traditionally implemented in synchronous

(dq), stationary (αβ), or natural (abc) reference frames and depending on the reference frame used the adopted control structures can be chosen from linear or nonlinear algorithms such as proportional integral (PI), proportional resonant (PR), vector control, hysteresis control, etc., [1]–[8].

The design simplicity and easier implementation of linear control algorithms used in synchronous or stationary reference frames have resulted in their relative popularity compared to nonlinear approaches. The synchronous reference frame which has received more attention uses a Park transformation to convert three-phase rotating quantities to direct and quadrature dc variables. These dc quantities can be regulated by using simple and linear PI controllers. Despite good performance in controlling dc variables, PI controllers have the well-known drawback of a nonzero steady state error; furthermore they fail to operate well in case of load changes and high penetration of DGs. in microgrids. Poor compensation capability for low-order harmonics has also been reported. Application of PR controllers in the stationary reference frame eliminates the steady state error, however, is accompanied with other drawbacks such as sensitivity to grid frequency variations, poor transient response during step changes, and low stability margins [9]. The use of natural reference frames on the other hand, requires more complex control structures such as hysteresis control. Application of such nonlinear structures will itself result in variable switching frequencies, which requires complex adaptive band hysteresis control [10]. In addition to classic control approaches, intelligent control algorithms such as fuzzy logic and artificial neural networks have been also used in recent years with the purpose of improving the transient performance and adaptivity; however, in most cases these algorithms increase the control system complexity [11]–[13].

The recently introduced proportional-resonant (PR) controllers and filters, and their suitability for current/voltage control of grid-connected converters, are described. Using the PR controllers, the converter reference tracking performance can be enhanced and previously known shortcomings associated with conventional PI

controllers can be alleviated. These shortcomings include steady-state errors in single-phase systems and the need for synchronous d–q transformation in three-phase systems. Based on similar control theory, PR filters can also be used for generating the harmonic command reference precisely in an active power filter, especially for single-phase systems, where d–q transformation theory is not directly applicable. Another advantage associated with the PR controllers and filters is the possibility of implementing selective harmonic compensation without requiring excessive computational resources.

Voltage-source converter (VSC)-based transmission systems have attractive potential features in terms of power flow control and stability of the network. Although relatively low switching frequency operation of high-power converters (9–15 times the line frequency) is desirable, it makes them sensitive to power network imbalances when they may be needed the most. Hence a control structure to improve the performance of high-power vector-controlled back-to-back VSC systems for conventional and emerging utility applications is proposed. The main improvement is to suppress the possible dc-link voltage fluctuations under power line faults and unbalanced conditions. The proposed controller structure is designed based on regulating the converter system's states locally in dq synchronous reference frame without sequence components extraction or resonant notch compensator. RTDS results verify the validity of the proposed control architecture during normal and unbalanced power system conditions.

In another method a vector control strategy for regulating the current of grid-tied voltage source converters in a rotating reference frame is discussed. The proposed approach is based on shaping the open-loop and closed-loop transfer matrices of the system. Solving a constrained convex optimization problem, the shaping is achieved, which guarantees the stability of the closed loop system. The designed controller results in the desired dynamic performance and decouples the direct and quadrature (dq) current axes. The structure of the proposed controller is similar to that of its predecessors and consists of four proportional-integral (PI) controllers.

Researches related to non-conventional energy sources have grown significantly in the present scenario. The electrical energy from the PV panel is considered as one of the most useful natural resources. The last method in this paper deals with the operation and control of a grid connected PV system with a nonlinear load. A utility grid connection is provided in order to replenish energy levels in case of power shortage from the renewable energy sources. Hysteresis Current Controller is employed for the inverter

control. The proposed inverter control technique interfaces renewable energy sources and the AC bus of micro grid. It offers the possibility to inject power from the renewable sources and also improves the power quality in the same micro grid.

II. DISCUSSION OF DIFFERENT METHODS FOR POWER CONTROL USING VSC'S IN MICROGRID

1. A Novel Self tuning PI Control system:

A novel self-tuning PI control system is proposed in this method to cope with the aforementioned deficiencies of traditional PI control by increasing the control system adaptivity while avoiding unnecessary complexity. To cope with the slow adaptation of traditional fixed-gain PI regulators to power changes, disturbances, and parameter variations a continuous scheme can be used to adjust the controller gains over time. The traditional solution is to tune the gains manually by observing the output of the system. However, to avoid unknown number of trial and error tasks in manual control and increase the reliability, an online and automatic tuning approach must be adapted. The authors have previously implemented a fuzzy system to automatically tune the gains of PI controllers in microgrids in [12]. In this method, no exact mathematical formula was used for the learning process, instead based on the reasoning capability of the fuzzy system the change in integral and proportional gains were estimated and used to tune the PI controller. In this paper, a novel gain-tuning algorithm is developed in which online tuning is achieved by combining the reasoning capability of a so-called fuzzy critic and a mathematical-learning algorithm. Critic based learning algorithms, also known as neuro-dynamic programming, are a wide group of learning methods that are usually used to facilitate the online tuning of intelligent controllers in case of highly nonlinear and noisy systems [13]. The proposed control system contains a PI controller and a critic agent whose task is to continuously assess the performance and generate an evaluation signal. The PI controller gains are updated using a learning algorithm with the objective of optimizing critic's output signal, which represents the credibility of the system performance. The proposed approach is a non model-based adaptive structure which will be named the critic-based self-tuning PI (CSPI) controller, hereafter in this paper. The CSPI controller is used to control the active and reactive power of VSCs within a power electronic-based microgrid.

2. Proportional Resonant Controllers:

Over the years, power converters of various topologies have found wide application in numerous grid-interfaced systems, including distributed power generation with

renewable energy sources (RES) like wind, hydro and solar energy, microgrid power conditioners and active power filters. Most of these systems include a grid-connected voltage-source converter whose functionality is to synchronise and transfer the variable produced power over to the grid. Another feature of the adopted converter is that it is usually pulse-width modulated (PWM) at a high switching frequency and is either current- or voltage-controlled using a selected linear or nonlinear control algorithm. The deciding criterion when selecting the appropriate control scheme usually involves an optimal trade off between cost, complexity and waveform quality needed for meeting (for example) new power quality standards for distributed generation in low-voltage grids, like IEEE-1547 in the USA and IEC61727 in Europe at a commercially favourable cost. With the above-mentioned objective in view while evaluating previously reported control schemes, the general conclusion is that most controllers with precise reference tracking are either overburdened by complex computational requirements or have high parametric sensitivity (sometimes both). On the other hand, simple linear proportional– integral (PI) controllers are prone to known drawbacks, including the presence of steady-state error in the stationary frame and the need to decouple phase dependency in three phase systems although they are relatively easy to implement. Exploring the simplicity of PI controllers and to improve their overall performance, many variations have been proposed in the literature including the addition of a grid voltage feed forward path, multiple-state feedback and increasing the proportional gain. Generally, these variations can expand the PI controller bandwidth but, unfortunately, they also push the systems towards their stability limits. Another disadvantage associated with the modified PI controllers is the possibility of distorting the line current caused by background harmonics introduced along the feed forward path if the grid voltage is distorted. This distortion can in turn trigger LC resonance especially when a LCL filter is used at the converter AC output for filtering switching current ripple [11, 12]. Alternatively, for three-phase systems, synchronous frame PI control with voltage feed forward can be used, but it usually requires multiple frame transformations, and can be difficult to implement using a low-cost fixed-point digital signal processor (DSP). Overcoming the computational burden and still achieving virtually similar frequency response characteristics as a synchronous frame PI controller, develops the P+ resonant (PR) controller for reference tracking in the stationary frame. Interestingly, the same control structure can also be used for the precise control of a single-phase converter. In brief, the basic functionality of the PR controller is to introduce an infinite gain at a selected resonant frequency

for eliminating steady state error at that frequency, and is therefore conceptually similar to an integrator whose infinite DC gain forces the DC steady-state error to zero. The resonant portion of the PR controller can therefore be viewed as a generalised AC integrator (GI), as proven in[10]. With the introduced flexibility of tuning the resonant frequency, attempts at using multiple PR controllers for selectively compensating low-order harmonics have also been reported in for three-phase active power filters, in for three-phase uninterruptible power supplies (UPS) and in for single phase photovoltaic (PV) inverters. From the view point that electronic power converters will find increasing grid-interfaced applications either as inverters processing DC energy from RES for grid injection or as rectifiers conditioning grid energy for different load usages, the information aims to provide a comprehensive reference for readers on the integration of PR controllers and filters to grid-connected converters for enhancing their tracking performances. To begin, the method reviews frequency domain derivation of the ideal and non-ideal PR controllers and filters, and discusses their similarities as compared to classical PI control.

It is desirable to have high-power high-voltage converter based systems available during power system faults when they may be needed the most. If the protection measures trip the converter system, it can take several fractions of an hour, depending on the size of the converter, to discharge the dc link and check the healthiness of the whole system. Hence, several practical methods have been proposed and implemented to keep a system operating under power system faults and disturbances. A voltage-source converter (VSC) is the main building block for flexible ac transmission systems (FACTS) devices and, as of today HVDC technology up to several hundred megawatts.

The increasing emergence of VSC-based transmission is the result of development in semiconductor devices, power electronic circuits, control, and executive engineering. Previously, the lack of these developments had prohibited the VSC-based technology from being the first choice. While each development is moving forward individually, the result of each one influences the design criteria and application requirements of the overall system. However, generally, less dependence on power semiconductor characteristics amounts to having more supplier possibilities for the VSC-based transmission. The most important limiting factor of power semiconductors is their switching properties since they are usually optimized for the conduction intervals. Hence, high-power electronic converters are desired to operate with relatively low switching frequencies (maximum9–15times the line frequency, and even lower for multilevel converters). The low switching frequency

operation of VSC systems imposes control limitations in case of power system faults and disturbances when they may be needed the most. To the best of the authors' knowledge, in the installed operating FACTS and HVDC systems, the ride-through capability is obtained either by proper passive element design [7], [8] or a change in the control mode [1]. On the other hand, with emerging high-power applications such as 10-MW wind generation turbines [9] or transportable recovery transformers [10], the dynamic operation of the VSC under power system disturbances must be revisited. This paper discusses an alternative control framework to obtain robust dc-link voltage with specific attention to design the VSC controller in the back-to-back (BTB) configuration,. The proposed controller is implemented in the dq (rotating) synchronous reference frame without sequence extraction.

3. Decoupled DQ-Current Control of Grid-tied Voltage Source Converters Using Nonparametric Models:

Voltage source converters (VSCs) are extensively utilized in many grid-tied applications while either their control system directly regulates their input current, or the adopted control system comprises an internal current feedback loop [7]. Therefore, the quality of the adopted current control strategy plays an important role in the overall performance of the system. Distributed power generation with renewable energy resources such as photovoltaic (PV) energy and wind energy, HVDC systems, active power filters (APF) etc, are some examples of such applications. Various current control approaches have been proposed for the grid-tied VSCs, which can be categorized into two major classes [1]: (i) linear and (ii) nonlinear controllers. Due to their structural simplicity and fully digital implement ability, linear approaches such as stationary reference frame (SRF) and rotating reference frame (RRF) controllers, are more commonly used. Among SRF controllers, proportional-resonant (PR) regulators are very well-known and popular. PR-controllers track AC references in the stationary frame with zero steady state error. However, they suffer from several drawbacks, e.g., sensitivity to grid frequency variations, exponentially decaying transients during step changes, and being pushed toward instability margins even by a small phase shift introduced by the adopted current sensors . Moreover, since PR-controllers have more poles than PI-controllers, they introduce a greater phase lag in the Nyquist plot of the open loop transfer function, which makes their tuning more complicated compared to PI-controllers. Furthermore, the choice of the damping ratio of the non-ideal PR-controllers, which are used in practice instead of ideal PR-controllers, is itself another design issue. Therefore, RRF-based controllers are normally preferred in many applications and show acceptable performance. Among RRF

controllers, PI-based regulators are the most renowned and easy-to-design ones, which provide fulfilling performance. The control scheme proposed in [10] is probably the most well-known and utilized approach in the literature. In this method, two current axes, i.e., direct and quadrature (dq)-axes, are defined, and a control strategy is proposed based on the mathematical model of the system. Using feed forward signals and PI regulators, the axes are independently controlled. However, due to imperfect disturbance rejection of PI-controllers, the parametric errors and the mathematical modelling mismatch result in coupled current axes. That is, upon a step change in each axis, the other axis experiences a transient, which results in power quality problems and performance degradation. Another RRF-based approach is proposed in whose structure is similar to that of the controller of , however, its axes decoupling capability is more efficient. This current control strategy is based on the pseudo-continuous model of the converter, and hereinafter, it is called the Pseudo-continuous Multivariable Current Controller (PMCC). Although the PMCC results in very sound performance, however, even adopting this approach, the current axes cannot be fully decoupled. The reason is that the PMCC also relies on the mathematical model of the system and the exact values of the system parameters. In this paper, it is shown that the parametric errors and modelling mismatch deteriorate the dynamic performance of the PMCC and result in the coupling of the dq-axes. The widespread applicability of the dq-current controller provides substantial inducements to investigate and propose alternative regulation schemes that can overcome the axes coupling problem. Using nonparametric models, this paper proposes a robust current regulation scheme for VSCs, in which the d and q-axes are decoupled. The design procedure consists of an optimization-based loop shaping, which guarantees the stability and the desired performance of the closed-loop system [8,9]. The structure of the achieved controller is similar to that of the PMCC [12], however, instead of integrators in the transversal arms of the controller, PI-controller are used. The proposed method provides better dynamic performance compared to its predecessors and is structurally simple.

III. RESULT ANALYSIS OF METHODS

1. A Novel Self tuning PI Control system

The CSPI controller is applied to the microgrid system shown in Fig. 1. Simulations are carried out in MATLAB/SIMULINK and to verify the feasibility of the proposed controller different operational scenarios in the grid connected mode and a case in islanded mode have been studied. To show the superiority of the CSPI algorithm compared to conventional PI control, the results from the

proposed controller are compared to those of traditional PI control in the first four cases. The PI coefficients are the best of the two sets of gains obtained from the Root Locus and Ziegler Nichols algorithms. The gains obtained from Root Locus algorithm resulted in a better response and then a manual tuning was employed to achieve to the best response.
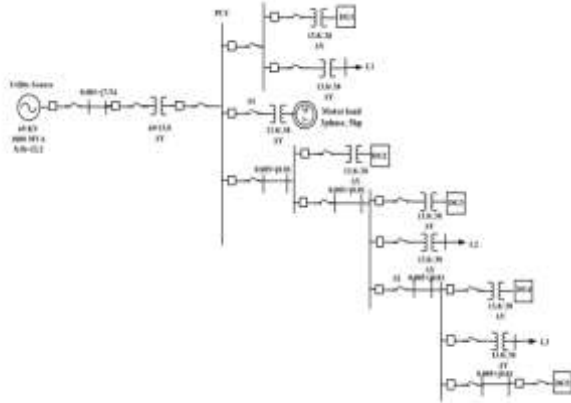

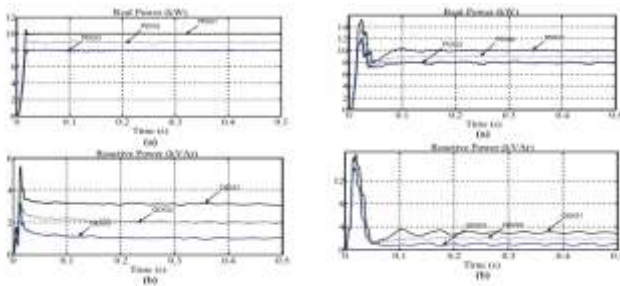Fig1:Single line diagram of microgrid system.

Case1: Grid connected microgrid:

Fig2: Real and Reactive power tracking under CSPI control over transient period
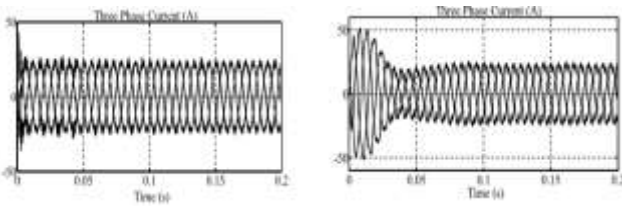
Fig3: Three phase current of DG1 under CSPI control & Three phase current of DG1 under PI control

As seen, in the CSPI control a smooth transient response is achieved and the output reaches its steady state within 0.02 s which is in the reasonable margin of 2–3 cycles for a power system and is almost one fourth of the transient time of 0.075 s in PI control. Also the initial power oscillations that are observed in PI control are completely removed for real power and significantly reduced for reactive power. It is worth noting that in practical microgrids

large power oscillations can lead to the unwanted activation of protection systems, in which case the microgrid DGs might fail to maintain the desired supply to loads. This can violate the overall system reliability and stability. Comparing both figures in fig. 2, it is evident that the proposed CSPI control achieves to a high level of harmonics attenuation compared to traditional PI control and the desired current shape is maintained.
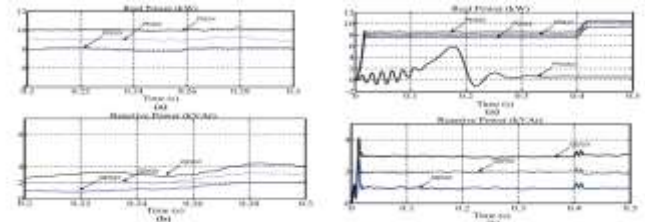
Case2: Islanded Microgrid:

Fig4: Real and reactive power under PI control & Real and reactive power under CSPI control.

zFig5:Three phase current in DG1 under PI Control & Three phase current in DG1 under CSPI control.

In the islanded microgrid, the CSPI controller is used in conjunction with frequency and voltage droops and an outer voltage control loop. As in this mode, the utility grid is not present, the major control tasks are voltage and frequency control. In the droop control, the frequency and voltage deviations are limited within a maximum allowed range to achieve proper active and reactive power sharing among multiple DGs. During the simulations switch S2, S1 and the switch at PCC are open and therefore an islanded 3-DG microgrid with two constant impedance loads rated at 15 kW and 3 kVAR is studied. As seen, the proposed CSPI controller results in significantly reduced initial power overshoot and steady state error; hence a faster and more accurate control is yielded.

2. PR Controllers and Filters.

Given the advantages of PR controllers and filters, a number of applications have since been proposed in the literature with most focusing on the control of converters interfaced directly to the utility grid. In this Section, one example case is presented for demonstrating the effectiveness of using PR controllers in a single-phase PV converter.

Single-phase PV grid-connected inverter

Single-phase grid inverters are commonly used in applications like residential RES (typically PV or fuel cell systems) and UPS. Figure shows a typical RES where the DC-link voltage, active P and reactive Q power are controlled in the outer control loops (labelled as voltage controller and

reference generator in the Figure). The reference current outputs of the outer loops (i_{dd}^+ and i^+) are next tracked by an inner current loop whose output is eventually fed to a PWM modulator for switching the inverter.

Typically, the inner current loop is implemented using a stationary PI current controller with voltage feed forward, as shown in Fig.6. Using PI control, however, leads to steady-state current error (both in phase and magnitude) when tracking sinusoidal input, and hence a poor harmonic compensation performance is expected [9]. Synchronous PI control can mitigate the tracking error, but is generally difficult to apply. Instead, the equivalent stationary PR controller can be used as the inner current controller, as shown in Fig. 10b. Compared to a stationary PI controller, the only computational requirement imposed by the PR controller is an extra integrator for implementing a second-order system, but with a modern low-cost 16-bit fixed-point DSP, this increase in computation can generally be ignored [9]. Besides that, using a PR controller would allow the removal of the grid voltage feed forward path, as proven in [9], and the simple cascading of a HC compensator for eliminating selected low-order harmonics.
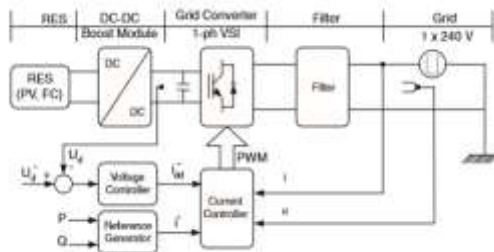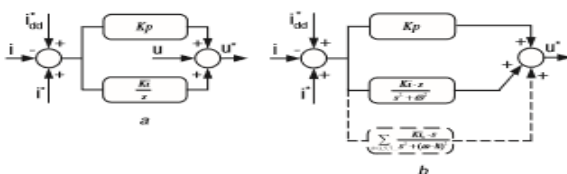

Fig6: Block diagram of typical single-phase RES system

Fig7: Single phase Grid Inverter control. a)Stationary PI control b)Stationary PR inner current control

The designed control scheme in Fig.6 has been tested using an experimental 3kW PV full-bridge inverter with an output LCL filter, as shown in Fig 5. The inverter is powered from a regulated DC power supply (set to $U_D=350V$) for simulating a PV string, and is interfaced to the utility grid with a voltage of Ug=230V RMS and a background THD of 1.46%. The resulting system is controlled digitally using a 16-bit fixed-point TMS320F24xx DSP platform with an execution time of 40 ms (including HC compensation) and the controller gains set as $K_p=2$, $K_i=300$ and $K_{ih}=300$ for h=3, 5 and 7. With these settings, the grid current and voltage at

50% load using PR and PR+HC controllers are shown in Figures. As seen in Fig., there is no phase error noted between the grid current and voltage, confirming the proper functioning of the PR controller. The harmonic distortion in Fig. 7 can be further reduced by cascading an HC compensator, as demonstrated by the smoother current waveform in Fig. 8.
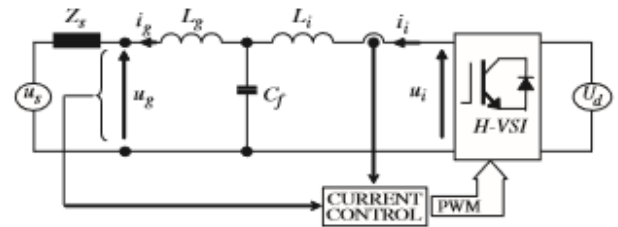

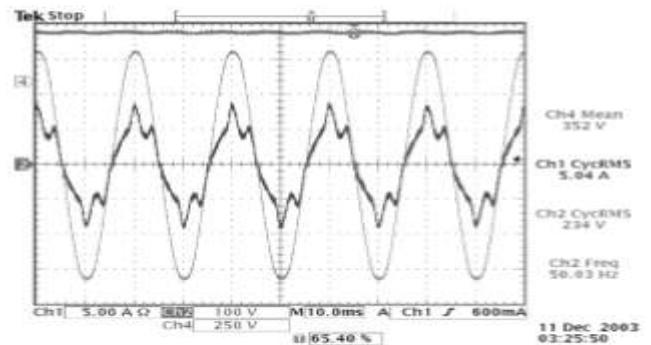Fig.8: Schematic Representation of experimental single phase PV Inverter.

Fig.9: Waveforms captured using PR controller at 50% load Grid voltage Ch2 [100V/div.], grid current Ch1 [5A/div.] and DC voltage Ch4 [250V/div.]
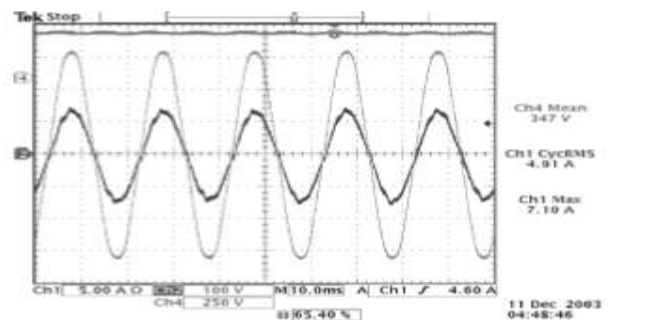

Fig.10: Waveforms captured using PR+HC controller at 50% load Grid voltage Ch2 [100V/div.], grid current Ch1 [5A/div.] and DC voltage Ch4 [250V/div.]

The improved performance achieved here with a single phase inverter can obviously be extended to a three-phase RES (e.g. small wind or water turbines and high-power PV plant).

3. Vector-Controlled Voltage-Source-Converters

This section presents and evaluates the dynamic performance of BTB VSC systems in different applications. Applications are categorized as HVDC, drive (wind), and hybrid power system applications. The proposed controller has been implemented in RTDS and compiled on a GPC processor card with a controller sampling time of 50μs and key circuit parameters as tabulated in Table.
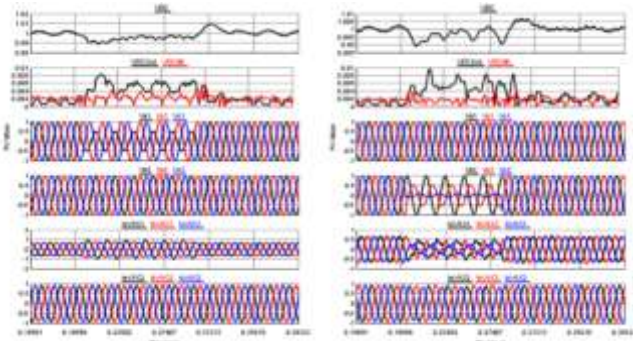

Fig.11: The unbalanced system is represented by a 50% voltage drop in phase A & the unbalanced system is represented by a 50% voltage drop in phase B

In Fig. 10, the unbalanced system is represented by a 50% voltage drop in phase A of the PCC voltages V_{abc1}.The fault remains for six cycles. A can be observed the dc-link voltage remains practically stiff, and harmonic measurement of the dc-link voltage for the second and fourth harmonics shows a satisfactory level of compensation. The inverter currents change (increase in phase A) to compensate for the unbalanced power flowing into the system; however, it remains within the safe operating area of the switches. In Fig. 11, the system performance under more severe imbalances is shown represented by a 50% and 90% voltage drop in phases B and C of the power flow controller side, respectively.
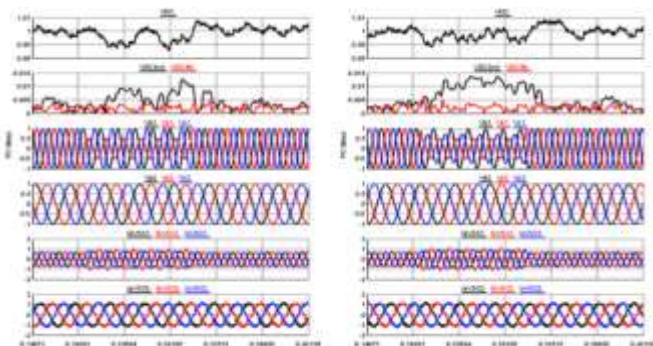

Fig.12: roller side and drive side operating at 30Hz.(RTDS results.) & Dynamic performance of the BTB VSC system in drive (wind) applications under an unbalanced condition of 50% in phase B and 30% in phase C voltage sag in the dc-link controller side (grid) and drive side operating at 30 Hz. (RTDS results.)

The dynamic performance of the VSC BTB system in the drive application under unbalanced conditions in the inverter side or grid side (dc-link voltage controller converter) is presented in Fig.11. The unbalance system is represented by 50% voltage drop in phase B of the inverter-side PCC. And a more severe fault occurs which is represented by a 50% voltage sag in phase B in addition to a 30% voltage drop in phase C of the grid. From the results obtained, it can be concluded that the proposed control scheme is effective in maintaining a robust dc-link voltage even under unbalanced grid conditions. In other words, the drive side in this case of high power wind generators with a BTB VSC interface can operate independently from the grid disturbances translating to higher availability of the renewable resources.
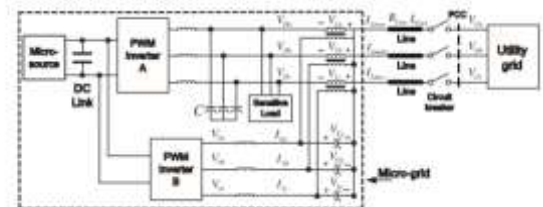

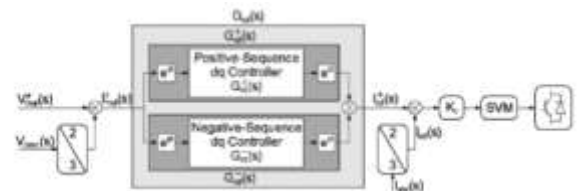Fig.13: Schematic of microgrid interfaced to utility grid using power quality compensator

Fig.14: Voltage control scheme of shunt inverter A

4. Decoupled DQ-Current Control of Grid-tied Voltage Source Converters Using Nonparametric Models

The Optimization-based Multivariable-PI Current Controller (OMCC) is based on minimizing the difference between the open-loop transfer matrix of the system and a desired open loop transfer matrix. The minimization is subject to some convex constraints and forms a convex optimization problem.

Performance Evaluation:

The purpose of this section is to evaluate the performance of the OMCC and also to compare it with that of the PMCC both in simulation and experiment. For the simulation part, the system of Fig.13, whose parameters are set according to Table I, is simulated in MATLAB/PLECS environment.
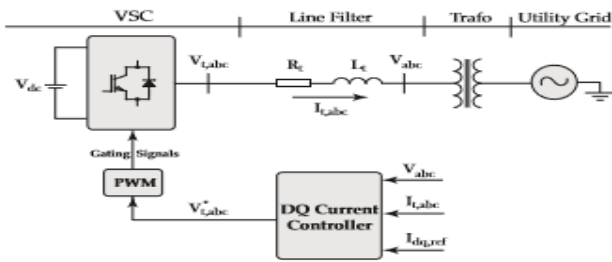
Fig.15: A one-line diagram of the three-phase test system.

TABLE1: Parameters of the three-phase test system

Quantity	Value	Comment
L_t	5 mH (0.18 pu)	Inductance of VSC Filter
R_t	0.3 Ω (0.036 pu)	Resistance of VSC Filter
VSC rated power	0.8 kW (1 pu)	$S_{base} = 0.8$ kVA
V_{dc}	350 V	DC Bus Voltage
V_s	230 V (rms) (1 pu)	Ph-G Grid Nominal Voltage
$n_1 : n_2$	5.4:1	Transformer Ratio
f_{sw}	5 kHz	PWM Carrier Frequency
f_s	5 kHz	Sampling Frequency
f	50 Hz	System Nominal Frequency
ω	314.15 rad/s	Nominal Angular Frequency

To convert the control and signal processing commands in discrete time, the bilinear method is used. The continuous time transfer functions are then transformed to discrete time and are developed into a S-function in MATLAB/Simulink. Moreover, for the experimental part, adopting the test system of Fig. 14 and the corresponding parameters of Table I, a three-phase experimental setup is implemented. To implement the control strategies and signal processing algorithms, an FPGA-based controller, which provides a C programming environment, is used. The adopted FPGA is XC4010PC84 FPGA manufactured by XILINX. The control and signal processing algorithms are first discretized using the bilinear method and then developed into C codes. It should be noted that in order to achieve perfect isolation between the power and control circuits, optic-based gate drivers are adopted for driving the IGBTs.

For the performance evaluation, a reference tracking test is conducted for each control strategy. Figs. 16 (a) and (b) depict the reference signals utilized in the conducted tests for the d and q-axes, respectively. $I_{t,d,ref}$ consists of three step changes, i.e., 0 to 10 A, 10 to 6 A, and 6 to 0 A, at the time instants t = 0.01s, t = 0.02s, and t = 0.045s, respectively. Moreover, $I_{t,q,ref}$ experiences two step changes from 0 to 8 A and from 8 to -10 A, at the time instants t = 0.03s and t = 0.055s, respectively. To design the PMCC, for the simulation, the parameters of Table I are adopted. Moreover, for the experimental part, the measured values of the resistance and inductance of the filter along with those of the transformer are used, which are measured by an RLC meter. The experimentally measured values comply with those of Table I. The difference between the measured value of R_t = 0.3 Ω

and the identified value of R_t = 1.1 Ω represents the parametric errors and also the un modeled resistive elements of the system. Therefore, to design the OMCC for the simulation and the experimental case, the simulation-based nonparametric model corresponding to R_t = 1.1 Ω and the experiment-based nonparametric model of Fig. 13 are adopted, respectively. Moreover, to mimic the experimental case in the simulation part, although the PMCC is designed for R_t = 0.3 Ω, R_t is set to 1.1 Ω in the simulated system. Of course, it must be noted that using a try and error approach, one can tune the PMCC to achieve better results and to reduce the error between the real value of R_t and the value used for the design. However, the purpose of this paper is to demonstrate the deficiencies of the PMCC, while systematically designed, compared to the OMCC. To design the controllers in the following sections, the same bandwidth is selected for all cases, which is ω_c = 1000rad/ s. Moreover, the weighting filter adopted for the OMCC design is $W_1(j\omega)$ = 0.5. This value guarantees a gain margin of at least 2 and a phase margin of greater than 29 degrees.
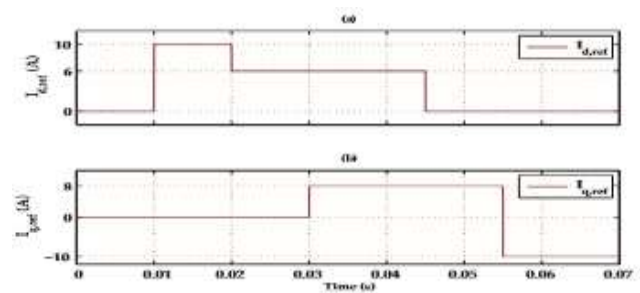

Fig.16: Reference value for the inverter current: a) d-component & b) q component

A. Simulation Results

In the simulation part, R_t is set to 1.1 Ω. However, in order to mimic the parametric errors of a real scenario, for the PMCC design, R_t is assumed to be 0.3 Ω. Then, adopting the aforementioned design parameters, the PMCC is designed, and it is represented by

$$\mathbf{K_{PMCC}}(z) = \begin{bmatrix} \frac{5.08z-4.92}{z-1} & -\frac{0.157z+0.157}{z-1} \\ \frac{0.157z+0.157}{z-1} & \frac{5.08z-4.92}{z-1} \end{bmatrix}.$$

Moreover, utilizing the simulation-based nonparametric model corresponding to R_t = 1.1 Ω and taking the aforementioned design procedure, the OMCC is designed, which is represented by

$$\mathbf{K_{OMCC}}(z) = \begin{bmatrix} \frac{5.089z-4.899}{z-1} & -\frac{0.320z+0.0001}{z-1} \\ \frac{0.320z+0.0001}{z-1} & \frac{5.089z-4.899}{z-1} \end{bmatrix}.$$
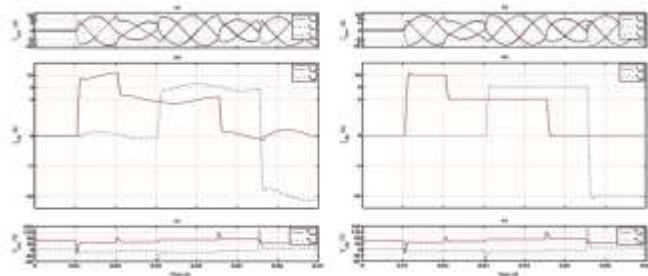
Fig.17: Simulation results of the transient response of the response PMCC during step changes in d- and d-axis: a) line currents, b) dq-component of the currents, and c) dq-components of and the control signals. & Simulation results of the transient of the OMCC during step changes a) line currents, b) dq-component of the currents, c) dq-components of the control signals.

In the following, the performance of the designed controllers of are respectively evaluated in simulation.

1) Reference Tracking Test for PMCC: In this section, adopting the aforementioned reference tracking test scenario in MATLAB/PLECS environment, the performance of the PMCC is evaluated. It is shown that due to the parametric errors and modeling mismatch, the dynamic performance of the PMCC deteriorates, and subsequent to step changes in the d-axis (qaxis), a non-negligible transient is experienced in the q-axis (d-axis). This verifies that the PMCC may not fully decouple the current axes. It must be noted that even if the parameters could be precisely determined, the modeling mismatch of the system, e.g., the modeling mismatch of the PWM converter, would result in slightly coupled current axes.

The test signals of Figs. 15(a) and (b) are applied to $I_{t,d,ref}$ and $I_{t,q,ref}$, respectively. Upon each step change, the line currents and their corresponding dq-components, as shown in Figs. 16 (a) and (b), change to track the reference signals in less than 2 ms with zero steady state errors. However, Fig. 16 (b) shows that upon each step change in each axis, the other axis experiences a transient whose magnitude depends on the amount of the step change and verifies that the PMCC suffers from axes coupling problem. Fig. 16 (c) depicts the dq-components of the control signals, which subsequent to each step change, are adapted to the new operating points by the PMCC.

2) Reference Tracking Test for OMCC: Utilizing the system of Fig. 1 equipped with the OMCC of and applying the test sequences of Figs. 15 (a) and (b) to $I_{t,d,ref}$ and $I_{t,q,ref}$, respectively, the same test is conducted for the OMCC to evaluate its performance. Subsequent to each change in the d- or q-axis reference value, the OMCC regulates the line currents at the desired level in less than 2 ms, as shown in Figs. 17 (a) and (b). Fig. 17 (b) depicts the dq-components of

the line currents, which subsequent to each step change, are regulated at the desired values as fast as the PMCC case and with zero steady state errors. Moreover, Fig. 17 (b) verifies that upon each step change in the d-axis(q-axis),the q-component(d-component)of the currents does not experiences any transient, which confirms the full axes decoupling capability of the OMCC. Fig. 17 (c) depict the dq-components of the control signals.

To numerically compare the decoupling capability of the controllers, the second norm of the error in d-axis during a step change in the q-axis is calculated. The utilized criterion is summarized as

$$d \;=\; \frac{1}{t_2 - t_1} \sqrt{\int_{t_1}^{t_2} e_q^2}.$$

. Calculating this norm for t1 = 0.055 s and t2 = 0.075 s, d = 3.82 for the PMCC, while d = 0.001 for the OMCC, which confirms more effective decoupling capability of the OMCC compared to that of the PMCC. Moreover, although the rise time of both controllers are the same, the OMCC settling time is much less than that of the PMCC. For example, subsequent to the last step change in the q-axis reference value, the OMCC reaches the ±5% steady state boundary within 2 ms while it takes 20 ms for the OMCC to reach that.

B. Experimental Results

In this section, the performance of the OMCC is experimentally evaluated and is compared with that of the PMCC. To design the PMCC, the filter parameters are of most importance and are measured using an RLC meter. The measured inductance and resistance of the line reactor filter and the transformer are L_t = 5.0 mH and R_t = 0.3 Ω, which are used to design the PMCC. However, to design the OMCC, the nonparametric model of the system is obtained through a PRBS-based identification on the experimental setup. Note that although the measured R_t is 0.3 Ω, however, the experiment-based identified nonparametric model complies with a theoretical model corresponding to R_t = 1.1 Ω.

The designed controllers in discrete time are represented by

$$\mathbf{K_{PMCC}}(z) = \begin{bmatrix} \frac{5.080z - 4.920}{z-1} & -\frac{0.157z + 0.157}{z-1} \\ \frac{0.157z + 0.157}{z-1} & \frac{5.080z - 4.920}{z-1} \end{bmatrix},$$

and

$$\mathbf{K_{OMCC}}(z) = \begin{bmatrix} \frac{5.140z - 4.851}{z-1} & -\frac{0.324z - 0.0004}{z-1} \\ \frac{0.324z - 0.0005}{z-1} & \frac{5.140z - 4.850}{z-1} \end{bmatrix}.$$

In the following, using the aforementioned reference tracking test, the performance of the designed controllers are experimentally evaluated.
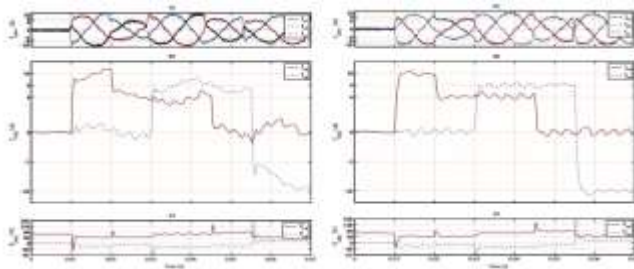

Fig.18: Experimental results of the transient response of the PMCC during step changes in d- and d-axis: a) line currents, b) dq-component of the currents, and c) dq-components of the control signals   & Experimental results of the transient response of the OMCC during step changes in d- and d-axis:a) line currents, b) dq-component of the currents and c) dq-components of the control signals.

1) Reference Tracking Test for PMCC: In this section, the performance of the PMCC is experimentally evaluated in terms of tracking reference signals. It is shown that in accordance with the simulation results, utilizing the PMCC, the dq-axes of the current are not fully decoupled, mainly due to the parametric errors and modeling mismatch.

To experimentally evaluate the performance of the PMCC, the reference tracking test is conducted. Figs. 17 (a) and (b) show the inverter current and their dq-components, respectively, which follow the step changes in the reference values in less than 2 ms. However, subsequent to each step change in the reference value of the d-axis (q-axis) current, the q-axis (d-axis) current experiences a non-negligible transient. Note that the dq components of the currents contain 300 Hz ripples, which are caused by the dead-time of the PWM strategy. Fig. 17 (c) shows the dq-components of the control signals that upon each step change, vary to accommodate the requested change. This results confirms that the PMCC may not fully decouple the axes due to the parametric errors and modeling mismatch.

2) Reference Tracking Test for OMCC: Utilizing the implemented experimental setup equipped with the OMCC and applying the same reference tracking test, the performance of the OMCC is experimentally evaluated. Fig. 17 (a) and (b) depict the line currents and their corresponding dq-components, respectively. Fig. 17 (b) shows that subsequent to each step change in the reference value of the d- or q-axis, the OMCC regulates the line currents at the desired level in less than 2 ms. Moreover, it confirms that upon a step change in each axis, the current of the other one remains unchanged. Fig. 17 (c) depicts the dq-

components of the control signals, which subsequent to each step change, are adapted to the new operating points by the OMCC.

The presented test results confirm the simulation results and show that the proposed controller, i.e., the OMCC, (i) is capable of tracking reference signals with zero steady-state errors, (ii) has fast dynamics, and (iii) contrary to the PMCC, provides fully decoupled d- and q-axes of currents.

Thus we can say that this method relies on shaping the nonparametric open-loop and closed-loop transfer matrices of the system through constrained convex optimization. The adopted constraints ensure the stability of the closed-loop system and also result in the desired performance.

5. Hysteresis Current Controller for a Microgrid Application

 a) System description.

Voltage source inverter based three phase grid connected inverter with control circuit is utilized in this paper. It acts as a shunt active power filter and is connected in parallel with the harmonic producing loads at the Point of Common Coupling (PCC). Configuration of the system is shown in Fig 1. Shunt active power filter generates a current equal and opposite to that of harmonic current drawn by the load and injects it at the point of common coupling making the source current sinusoidal. Filtering algorithm used and calculation of load current harmonics decides the characteristics of harmonic compensation. Reference current extracted by Synchronous reference method is compared with the filter current in the hysteresis loop and corresponding pulses are given for inverter switching. Inductor provides smoothing and isolation of high frequency components. Desired current waveform is obtained by controlling the switching of IGBT switches in the inverter. A nonlinear load of 10 kW is connected to a three phase source of 415 V. PV system with a capacity of 3.3 kW is interconnected to the grid through an inverter. PV system is equipped with MPPT control, DC-DC converter and a bidirectional inverter.
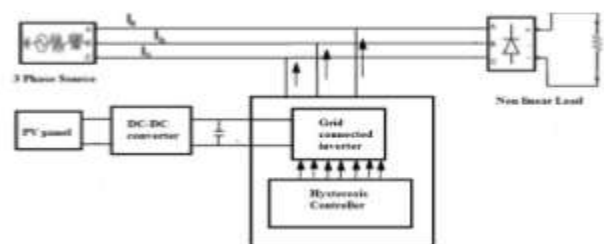

Fig.19: System Configuration.

b) Simulation Results:

The PV system is modeled using MATLAB Simulink platform. Table2 shows the parameter details of a PV panel.

Table 2 Parameter details of a PV panel

Parameter	Set Value
Rated output Power	220 W
Short circuit current	10 A
Open circuit voltage	22.2V
Current at maximum power	9.9 A
Voltage at maximum power	17.2 V
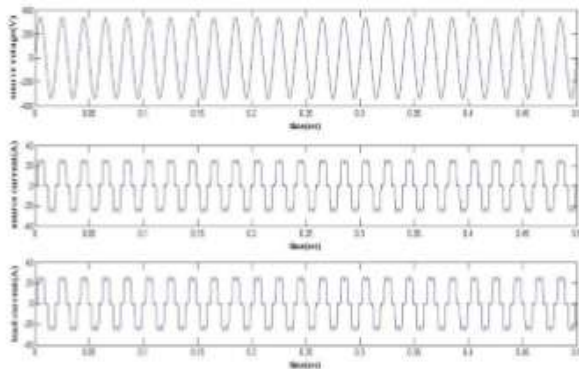
Fig.20: Waveform of source voltage, source current, load current

The PV system with MPPT control algorithm is integrated to grid with hysteresis current controller with same nonlinear load of 10 kW. Real power sharing, harmonic elimination and power factor improvement are analyzed. The current waveform after the compensation is shown in fig 19.
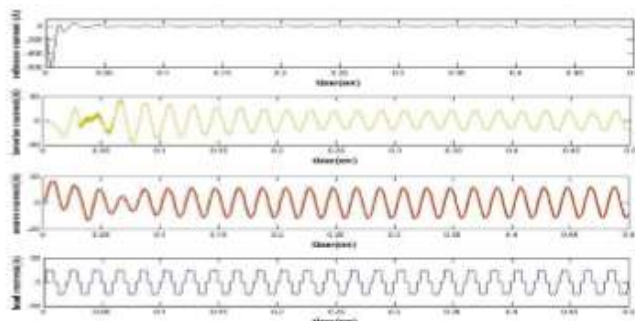

Fig.21: current waveform after compensation

It is inferred that PV system and grid shares the load and also the harmonics in the source current are eliminated.

The source voltage and current waveform for power factor analysis is shown in fig 21. Power factor is improved after a delay of 0.15 seconds.
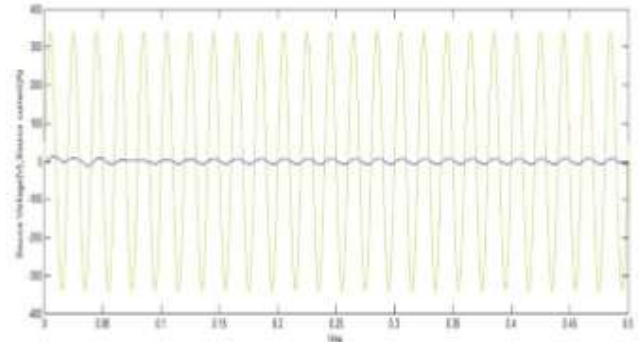

Fig.22: Power factor improvement

When an additional load of 5 kW is added to the system at 0.4 sec, grid provides the power required for the additional load since maximum capacity of PV generator has reached. Fig 22 shows the power sharing between PV and grid.
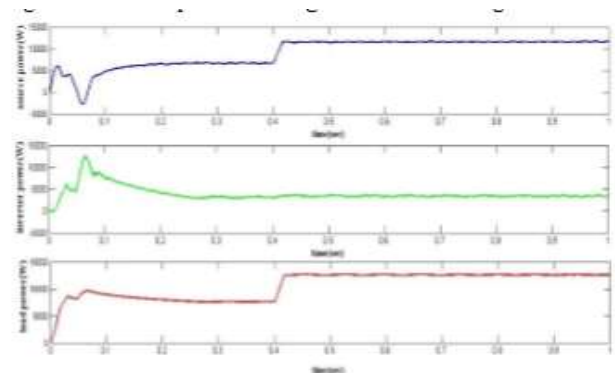

Fig.23: Power sharing when additional load of 5 kW is added

When the nonlinear load connected to the system is 1200W, the PV itself can support the load. So no power is drawn from the grid. The fig 23 shows the power sharing waveform when the load is 1200 W.
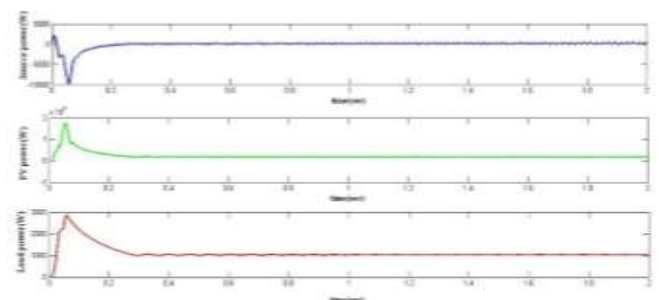

Fig.24: power sharing waveform when load demand is 1200 W

If any unfavorable situation occurs, ie, when there is no supply from PV generators, the grid supports the entire load demand. The power sharing of the system in the absence of PV   is shown in fig 24.
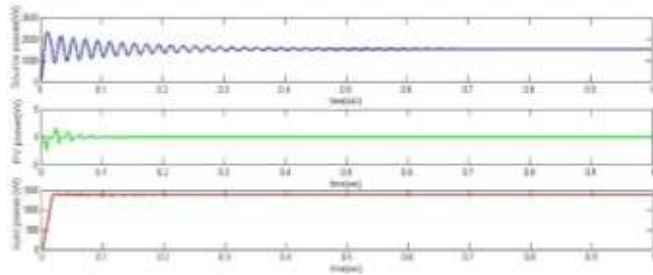
Fig.25: Power sharing in the absence of PV system

From the simulation done for the various conditions of load, it is found that the THD of system source current is improved from 26.62% to 3.84% after compensation. The PV system was capable of injecting 3.2 kW power to the system.

IV. CONCLUSION

Thus we have discussed different types of strategies and methods of controlling power in Voltage Source Converter based Microgrid power system. In CSPI based controller the results verify the effectiveness of the proposed algorithm and prove that the CSPI controller has significantly improved the microgrid performance by reducing the convergence time, power oscillations, and tracking error especially in case of higher DG penetrations. Implementation wise, the PR technique requires lesser computational overhead and does not require an explicit grid voltage feed forward control path, while still achieving the same performance as a synchronous PI controller. The vector controlled VSC's obviates the need for the sequence extraction blocks or the resonant compensators. Therefore, there is no diminishing bandwidth factor. The RTDS verification of the controller attained less than 1% dc-link voltage deviation under most common faults and disturbances. The proposed optimization-based method tracks the reference signals with zero steady state errors, has better dynamic performance compared to the previously proposed approaches and results in decoupled current axes. Lastly in Hysteresis current controller based system the PV system is tested and results confirm better real power sharing, power factor improvement and harmonic elimination.

V. REFERENCES

[1] M. Prodanovic and T. C. Green, "Control and filter design of three-phase inverters for high power quality grid connection," IEEE Trans. Power Electron., vol. 18, no. 1, pp. 373–380, Jan. 2003

[2] N. Kroutikova, C. A. Hernandez-Aramburo, and T. C. Greean, "Statespace model of gridconnected inverters under current control mode," IET Elect. Power Appl., vol. 1, no. 3, pp. 329–338, 2007.

[3] K. Sao and P. W. Lehn, "Control and power management of converter fed microgrids," IEEE Trans. Power Syst., vol. 23, no. 3, pp. 1088–1098, Aug. 2008.

[4] C. Schauder and H. Mehta, "Vector analysis and control of advanced static VAr compensators," IEEE Proc. C Gen. Transmiss. Distrib., vol. 140, no. 4, pp. 299–306, Jul. 1993.

[5] F. Katiraei and M. R. Iravani, "Power management strategies for a microgrid with multiple distributed generation units," IEEE Trans. Power Syst., vol. 21, no. 4, pp. 1821–1831, Nov. 2006

[6] N. Pogaku, M. Prodanovic, and T. C. Green, "Modeling, analysis and testing of autonomous operation of an inverter-based microgrid," IEEE Trans. Power Electron., vol. 22, no. 2, pp. 613–625, Mar. 2007.

[7] D. N. Zmood and D. G. Holmes, "Stationary frame current regulation of PWM inverters with zero steady-state error," IEEE Trans. Power Electron., vol. 18, no. 3, pp. 814–822, May 2003.

[8] R. Teodorescu, F. Blaabjerg, M. Liserre, and P. C. Loh, "Proportionalresonant controllers and filters for grid-connected voltage-source converters," IEE Proc. Elect. Power Appl., vol. 153, no. 5, pp. 750–762, Sep. 2006.

[9] G. Shen, X. Zhu, J. Zhang, and D. Xu, "A new feedback method for PR current control of LCL-filter-based grid-connected inverter," IEEE Trans. Ind. Electron., vol. 57, no. 6, pp. 2033–2041, Jun. 2010.

[10] F. Blaabjerg, R. Teodorescu, M. Liserre, and A. V. Timbus, "Overview of control and grid synchronization for distributed power generation systems," IEEE Trans. Ind. Electron., vol. 53, no. 5, Oct. 2006, pp. 1398–1409

[11] G. K. Venayagamoorthy, "Potentials and promises of computational intelligence for smart grids," in Proc. IEEE Power Energy Soc. Gen. Meeting, Calgary, AB, Canada, Jul. 2009, pp. 1–6.

[12] G. Rami, T. Tran-Uoc, and N. Hadjsaid, "Fuzzy logic supervision and control of distributed generators," in Proc. 18th Int. Conf. Exhibit. Elect. Distrib. (CIRED), Turin, Italy, 2005, pp. 1–5.

[13] N. L. Diaz, F. H. Barbosa, and C. L. Trujillo, "Analysis and design of a nonlinear fuzzy controller applied to a VSC to control the active and reactive power flow," in Proc. Electron. Mech. Autom. Conf., 2007, pp. 417–422.